Nanoscale-to-Mesoscale Heterogeneity and Percolating Favored Clusters Govern Ultrastability of Metallic Glasses

Qiang Luo,* Zhengguo Zhang, Donghui Li, Peng Luo, Weihua Wang, and Baolong Shen*

Cite This: https://doi.org/10.1021/acs.nanolett.1c05039

Read Online

ACCESS | Metrics & More | Article Recommendations | SI Supporting Information

ABSTRACT: Comprehending and controlling the stability of glasses is one of the most challenging issues in glass science. Here we explore the microscopic origin of the ultrastability of a Cu−Zr−Al metallic glass (MG). It is revealed that the ultrastable window ($0.7-0.8\ T_g$) of MGs correlates with the enhanced degree of nanoscale-to-mesoscale structural/mechanical heterogeneity and the connection of stability-favored clusters. On one side, the increased fraction of stability-favored clusters promotes the formation of a stable percolating network through a critical percolation transition, which is essential to form ultrastable MG. On the other side, the enhanced heterogeneity arising from an increased distribution in local clusters may promote synergistically a more efficient and frustrated packing of amorphous structure, contributing to the ultrastability. The present work sheds new light on the stability of MGs and provides a step toward next-generation MGs with superior stability and performances.

KEYWORDS: Metallic glasses, ultrastability, heterogeneity, percolation transition
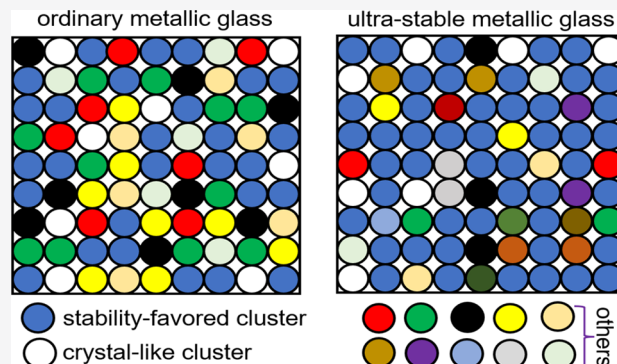
Glasses undergo natural aging during storage and crystallization upon continuous heating. Understanding and enhancing the stability against aging and crystallization of glasses are of significance not only for fundamental science but also for performance and reliability in applications.[1−3] Recent experiments demonstrate that glasses created by vapor deposition show extraordinary stability and many attractive properties compared with liquid quenched glasses.[3−11] Usually, ultrastable glasses can be created in a relatively low depositing rate within a narrow deposition temperature (T_{sub}) range below T_g (T_g is the glass transition temperature of a liquid quenched glass).[12−15] This optimal temperature differs slightly in different kinds of glasses, locating around $0.7-0.8\ T_g$ for some metallic glasses (MGs), and about $0.8-0.9\ T_g$ for many organic glasses.[1,7,12−14] The correlations between ultrastability with Kauzmann temperature and Johari−Goldstein β-relaxation were suggested.[7,15] However, the microscopic mechanisms ruling the ultrastable window of $\sim 0.7-0.9\ T_g$ are not well understood even for MG systems without complex inter- and intramolecular interactions.[16−20] Besides, it was reported that ultrastability cannot be obtained in some Zr-based MGs.[16,17] This composition-selected ultrastability is a mystery in MG systems.

Here we explore the correlation between stability and nanoscale-to-mesoscale structural/mechanical heterogeneity of $Zr_{46}Cu_{46}Al_8$ MGs. It is observed that the crystallization temperature (T_x) increases vastly from 755 to 875 K when the T_{sub} increases from 298 to 560 K ($0.80\ T_g$). But when

deposited at 596 K ($0.85\ T_g$), the obtained MG shows a massive decrease of T_x to 667 K. By using start-of-the-art structure characterizations, we unveil that combined effects of the moderately enhanced heterogeneity arising from increased dispersity of structural units and the formation of a percolating network of stability-favored clusters are crucial to forming ultrastable metallic glass (UMG). The ordinary-ultrastable transition of stability in MGs can be considered as a percolation transition of stability-favored clusters. Moreover, distinct relaxation behaviors of the nanoscale-to-mesoscale heterogeneity have been observed between the UMG and ordinary MG.

Figure 1 depicts the in situ X-ray diffraction (XRD) patterns measured at different temperatures for the MGs deposited at 298, 560, and 596 K (later denoted as MG-298, MG-560, and MG-596, respectively). All the XRD patterns of the as-deposited MGs show amorphous characteristics, with a small peak around $\sim 28°$ from the Pt sample holder. The amorphous nature can be further seen from the TEM images and their corresponding FFT patterns (Figure S1). Despite similar TEM
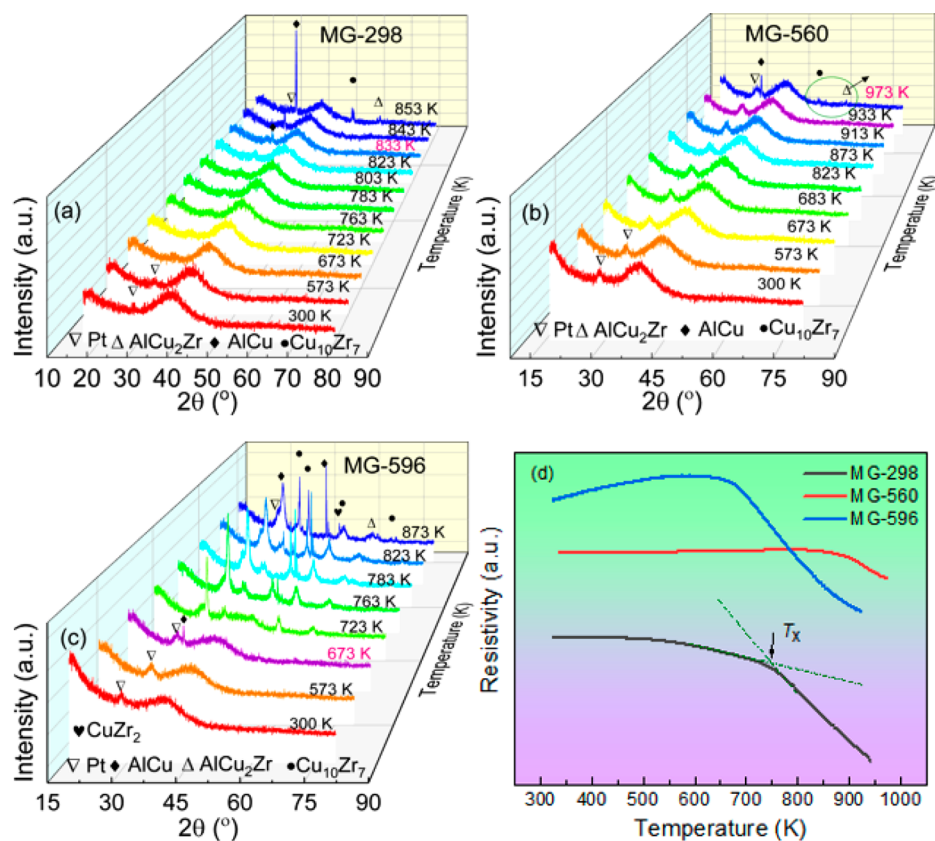
Figure 1. (a–c) In situ XRD patterns. (d) Temperature dependence of the resistivity.

features, these MGs exhibit vastly different thermal stabilities against crystallization. MG-298 remains amorphous in 300–823 K within the resolution limit of XRD (Figure 1a), and a crystalline peak appears at 833 K. In contrast, no crystalline peak can be observed below and at 933 K (Figure 1b) for MG-560, and some crystalline peaks are detected at 973 K, implying a much higher T_x. However, some crystalline peaks are observed from 673 K for MG-596 (Figure 1c), indicating its worst stability. The resistivity measurements with continuous heating are further carried out to detect the crystallization event. As shown in Figure 1d, the resistivity of MG-298 shows a sudden considerable reduction around 755 K due to crystallization. This $T_x \sim 755$ K is similar to that observed by another publication.[19] The MG-560 and MG-596 samples show the largest $T_x \sim 875$ K and lowest $T_x \sim 667$ K, respectively. These results are consistent with the XRD results.

Next, we investigated the mechanical heterogeneity at the nanoscale and the mesoscale in the MGs by using the image ability of the KLA Tencor G200. Figure 2a presents the 3-D map of contact stiffness of the as-deposited MG-560 as an example, showing apparent heterogeneity. Under the same conditions, the average contact stiffness values are 8661.7, 9149.7, and 8860.5 N/m for MG-298, MG-560, and MG-596, respectively, showing a similar T_{sub} dependence of the hardness and modulus (Figure S4). To illustrate quantitatively the different degrees of mechanical heterogeneity, the stiffness distribution has been determined and is shown in Figure 2b. The full width at half-maximum (FWHM) is determined to be 6.6%, 11.0%, and 19.2% for MG-298, MG-560, and MG-596, respectively. It is striking that increasing T_{sub} enhances the mechanical heterogeneity instead of homogeneity. This indicates that the enhanced surface mobility at a high T_{sub}
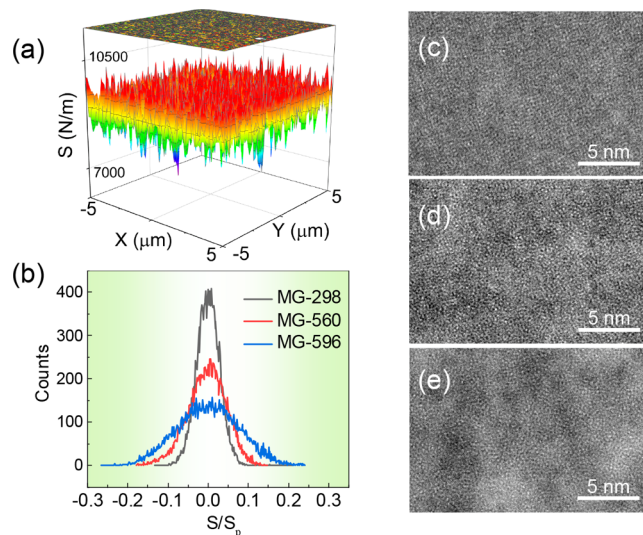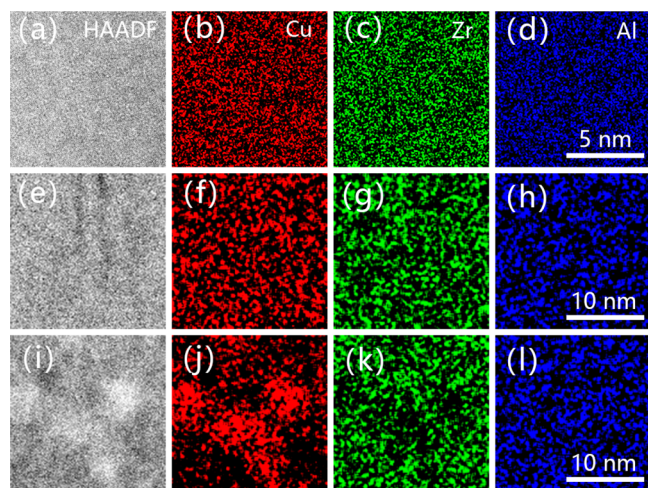

Figure 2. (a) 3-D image of the contact stiffness for MG-560. (b) Distribution of the contact stiffness for the MGs. HAADF-STEM images of (c) MG-298, (d) MG-560, and (e) MG-596.

causes more diverse distributions of clusters in present system. Besides, viscoelastic heterogeneity is also observed in all the MGs (Figure S3),[21] and the largest hardness and indentation modulus are obtained in MG-560 (Figure S4) due to its reduced free volume and unique packing of clusters.[22,23]

To reveal the structural origin of the variations of stability and mechanical heterogeneity with T_{sub}, the atomic structure has been investigated by aberration-corrected high-angle annular dark-field scanning transmission electron microscopy

(HAADF-STEM). All the MGs show heterogeneous contrast with dark and bright domains at the nanoscale, as seen in Figure 2c−e, indicating an inhomogeneous distribution of density and/or chemistry. The spatial heterogeneity, as an intrinsic characteristic of MGs,[24−28] plays an important role in vibration/relaxation, deformation, and glass formation.[29−38] But the correlation between atomic heterogeneity and ultrastability is elusive. The high-resolution HAADF-STEM images in Figure 2 unveil that the UMG has an enhanced degree of heterogeneity at the nanoscale (Figure 2d) compared with that of MG-298 (Figure 2c). Increasing T_{sub} from 560 to 596 K leads to a further increased heterogeneous contrast (Figure 2e) but considerably worsens the thermal stability. These results suggest that controlling the nanoscale heterogeneity is important to enhance stability. In a rapidly quenched Zr−Cu−Al MG, the dark and bright domains observed in the HAADF-STEM images are revealed to arise from the clusters with crystal-like and icosahedron-like orders, respectively.[32] Therefore, it is reasonable to argue that bright and dark domains with the nanometer scale in the HAADF-STEM images of MG-298 and MG-560 in Figure 2 originate from different medium-range-order (MRO) clusters with distinct symmetries and densities.
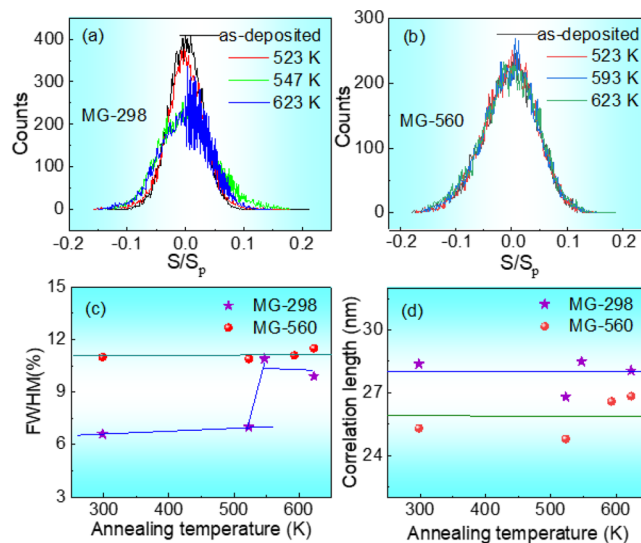
To check whether the observed heterogeneous contrast in Figure 2c−e partly arises from chemical fluctuation, STEM-EDS mapping has been conducted, and the results are shown in Figure 3. For MG-298 and MG-560, it is impossible to
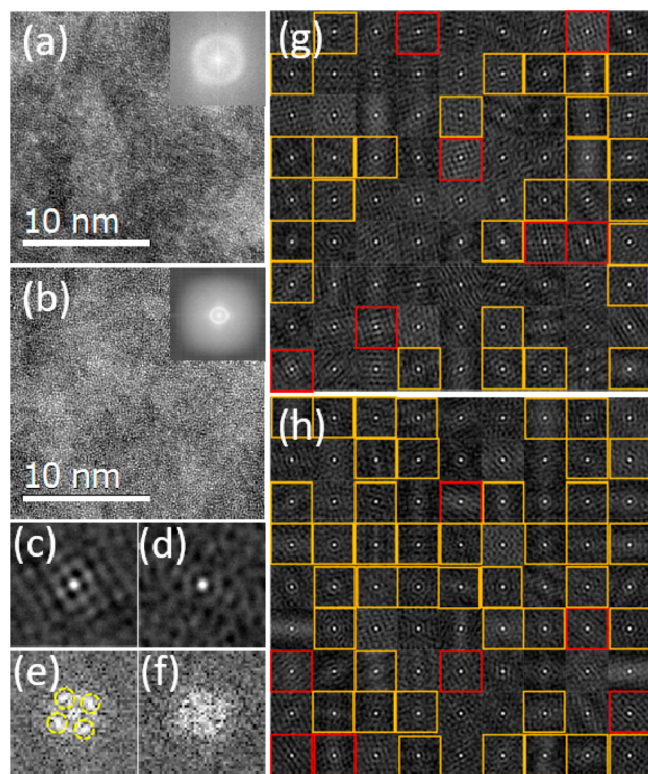
Moreover, the structural/mechanical heterogeneity of MG-298 and MG-560 (UMG) shows distinct responses to annealing. As presented in Figure 4a, the statistical distribution

Figure 4. Distribution of the contact stiffness for the as-deposited and annealed MG-298 (a) and MG-560 (b). (c) FWHM of distribution for the as-deposited and annealed MGs. (d) Correlation length of the stiffness images for the as-deposited and annealed MGs.

of stiffness becomes slightly changed after annealing at 523 K (0.75 T_g) for 120 min but broadens obviously after annealing at 547 K (∼0.78 T_g). This obvious change of mechanical heterogeneity may relate to the apparent change of the MRO and β-relaxation process.[43] The FWHM can be determined to be 7.0%, 10.9%, and 9.9% for the MGs annealed at 523, 547, and 623 K (0.89 T_g), respectively. In contrast, the stiffness distribution curves show little change for the as-deposited and annealed MG-560, as seen in Figure 4b, with the FWHM of around 11.0%, indicating the suppression of the clusters' rearrangements during annealing. It is interesting to note that with increasing annealing temperature, the FWHM of MG-298 tends to approach that of the UMG (Figure 4c). In addition, the correlation length of the stiffness heterogeneity for both MG-298 and MG-560 shows little change after annealing, as indicated in Figure 4d. Note that MG-560 shows smaller correlation lengths than MG-298, which may be associated with its larger mechanical heterogeneity and denser structure.

The HAADF-STEM observation has been performed for MG-298 and MG-560 annealed at 547 K for 200 min to reveal the structural origin of the mechanical heterogeneity change. From Figure 5a and Figure 2c, the structural heterogeneity at the MRO scale of MG-298 increases obviously after annealing. Differently, no apparent change of heterogeneous contrast in the STEM images can be detected for the annealed MG-560, as seen from Figure 5b and Figure 2d. The similar change trends of STEM heterogeneity and stiffness distribution upon annealing in MG-298 and MG-560 indicate that the mechanical heterogeneity correlates well with and arises from atomic heterogeneity at the MRO scale. More detailed local structure changes upon annealing can be revealed from the autocorrelation analysis of the HAADF-STEM images, which can evaluate the degree of structural order.[39] The HAADF-STEM image is divided into 81 square cells with a length of 1.993 nm, which is the typical size of the MRO in MGs.[24,28]

Figure 3. EDS mappings of each element and the corresponding HAADF-STEM images of MG-298 (a−d), MG-560 (e−h), and MG-596 (i−l).

detect the visible chemical variation correlated with the heterogeneity (Figure 3a−h). In contrast, MG-596 presents the most inhomogeneous distributions of Cu/Zr atoms (Figure 3i−k), and a relatively homogeneous distribution of Al atoms (Figure 3l). Especially in Figure 3j, the aggregation of Cu atoms is clearly observed at the scale of a few nanometers, which forms at the cost of Cu deficiency in the surrounding areas (Figure 3k). A combination of the STEM image and EDS map of Cu indicates that the bright domains in the STEM image correspond to the Cu-rich (Zr-poor) regions of the EDS map. This means that the structural heterogeneity of MG-596 mainly comes from nanoscale compositional fluctuations of Cu/Zr with a secondary contribution from the change of distribution in the MRO clusters.

Figure 5. (a, b) HAADF-STEM images of MG-298 K and MG-560 K annealed at 547 K for 200 min, respectively. The insets are the FFT patterns. (c, d) Autocorrelation images of the typical type A and type B cells, respectively. (e, f) FFT patterns of cells from (c, d), respectively. (g, h) Autocorrelation maps of as-deposited MG-298 and MG-560, respectively.

From the autocorrelation maps, two kinds of cells (with the two extreme degrees of structure order in MGs) can be well identified as illustrated in Figure 5c,d. One is the type A, like Figure 5c, showing a clear fringe of crystal-like order (the corresponding FFT pattern in Figure 5e shows diffraction spots). Another kind of cell (type B) presented in Figure 5d shows the most disordered maze-like feature with an inner circular-like fringe (the corresponding homogeneous FFT pattern is shown in Figure 5f), indicating the most disordered local structure. All the other cells that cannot be well-defined are denoted as type C. We have marked the type A and type B cells by red and yellow boxes, respectively, in the autocorrelation maps of the as-deposited MG-298 (Figure 5g transformed from Figure 2c) and MG-560 (Figure 5h from Figure 2d) and the annealed MG-298 (from Figure 5a) and MG-560 (from Figure 5b) in Figure S9. For both MG-298 and MG-560, the total area fraction of the crystal-like-order domains increases from $8.6 \pm 2\%$ to $11.1 \pm 2\%$ after annealing, and the fraction of type B domains decreases slightly. Moreover, it is noted that the fraction of the type B domains in as-deposited MG-560 is $51.9 \pm 2\%$, which is much larger than $32.1 \pm 2\%$ of as-deposited MG-298. This indicates that the type B clusters, as the stability-favored clusters, dominate the ultrastability of MG-560. And the little change of the stiffness distribution upon annealing in MG-560, reflecting the mechanical stability at the scale of a hundred nanometers, may correlate with its high fraction of type B clusters.

It is well accepted that the formation of ultrastable glasses is related to the enhanced surface dynamics, which helps atoms

find near-equilibrium configurations. From simulations, the ultrastable glasses for Lennard-Jones systems have been revealed to show a more-uniform packing arrangement with smaller amplitude density fluctuations than the ordinary glasses.[7,20] However, the present work uncovers a novel UMG state with a more heterogeneous packing at the nanoscale and the mesoscale. Thus, it seems that the complex energy landscape of MG systems possesses different ultrastable states with different heterogeneities.[19,20] For the present MG system, the enhanced heterogeneity relates to the distribution changes of the types B and C clusters (Figure 5), forming a stable and complex cluster network. In MGs, solute-centered clusters are densely packed to constitute different types of the MRO (such as fcc- and icosahedral-like MROs),[24−28] which form a fractal network.[26] Notably, in Cu−Zr MG systems, simulations reveal that a significant fraction of the icosahedral cluster exists, forming an interpenetrating string-like backbone network.[31,33,34] It is possible that most of the type B cells are icosahedron-like clusters, which are energetically and geometrically favorable and long-lived. The significantly enhanced fraction of type B clusters in the UMG is according to a simulation work, which reveals that the UMG has a higher fraction of icosahedral-like clusters than the liquid quenched MG.[20] We argue that the formation of a percolating network of stability-favored clusters is the key to achieve ultrastability. A similar percolating model has been used to illustrate the glass transition of MG.[25] The basic idea of percolation model widely used in disordered conductor/insulator composites is illustrated in Figure S10a,b, considering the change of property with probability of occupied (p) and empty ($1 − p$) sites. At low p values, the system is insulated due to the poor connection. A percolating network can form above the percolation threshold (p_c), permitting conduction. In Figure 5g,h, the packing fraction (ϕ) of the type B cell corresponds to p, and the percolation threshold corresponds to a critical volume fraction (ϕ_c). From Figure 5h, MG-560 has a considerably higher fraction ($51.9 \pm 2\%$) of stability-favored clusters than MG-298 ($32.2 \pm 2\%$), which naturally leads to formation of a stable percolating backbone network (Figure 5h) permitting ultrastability. Types A and C clusters are mainly surrounded by the percolating stability-favored clusters that act as an impediment for further aggregation and growth of types A and C clusters,[18] stabilizing the structure of the UMG most efficiently. Differently, type C ($59.3 \pm 2\%$) instead of type B clusters (Figure 5g) form a less stable percolating network in MG-298. From the above results, the percolation threshold of type B clusters should locate between $32.1 \pm 2\%$ and $51.9 \pm 2\%$ to create UMG. For MG-596, the nanoscale compositional fluctuations of Cu/Zr decrease the thermal stability in two aspects. First, it influences the distribution of clusters and especially decreases significantly the fraction (∼20%) of the stability-favored clusters (Figure S11), breaking up the percolating stable network. Second, the atom segregation may act as a precursor of crystallization, further decreasing the thermal stability.

The percolation model not only can explain naturally the tremendous change of crystallization temperature as a function of T_{sub} but also can illustrate why in some MGs ultrastability cannot be obtained.[16,17] Maybe in these systems, there exists only a few icosahedron-like clusters, which cannot form a stable percolation network. Moreover, the transition from ordinary stability to ultrastability with distinct network structures and mechanical properties in the present MGs

implies a novel glass-to-glass transition driven by varying T_{sub}, just as suggested in an organic glass.[40] Note that in the Cu−Zr (Al) systems, liquid-to-liquid transitions with a distinct change of local structures have been reported from viscosity measurements.[41,42] In the $Zr_{46}Cu_{46}Al_8$ MG ribbon, an annealing-induced transition of the MRO has been observed,[43] indicating the sensitivity of the MRO to temperature in Cu−Zr−Al system. But the correlation between the liquid−liquid transition and the present percolation transition from ordinary MG to UMG remains to be settled.

Besides, the enhanced structural heterogeneity in the UMG implies the increased distribution of clusters. This is further supported from the XRD results, which show a larger full-width at half-maximum of the first peak for the UMG (11.6° and 13.8° for MG-298 and MG-560, respectively). Thus, the UMG has a more disordered structure with a shorter correlation length.[24−26] Recently, it has been found that a larger full-width at half-maximum of the first peak in the XRD pattern relates to a larger distribution of local clusters, which results in efficient packing of local structure and thus enhanced glass forming ability.[44] Likewise, we argue that the increased structural heterogeneity contributes undeniably to the ultra-stability by enhancing synergistically the dispersity of local clusters in UMG and promoting a more efficient and frustrated packing of clusters. In addition, the moderately enhanced mechanical heterogeneity arises directly from dispersity of local clusters in UMG.

MG-298 evolves toward a more structurally/mechanically heterogeneous state upon annealing, which is akin to the rejuvenation effect (realized by shot-peening, temperature cycling, etc.) associated with the enhanced structural heterogeneity.[45−47] In the $Zr_{50}Cu_{40}Al_{10}$ MG, the rejuvenation effect has been observed after elastic loading, which correlates with the increased fluctuations of elastic modulus.[38] Usually, two mechanisms ruling physical aging are considered: an irreversible atomic rearrangement with density changes and a reversible one relating to the change of short-range order but without density change.[48−50] Particularly a secondary relaxation process without volume reduction ($T/T_g \geq 0.79$ for the $Pd_{77}Si_{16.5}Cu_{6.5}$ MG) arising from thermal activation of atomic rearrangements in the medium-range order has been revealed.[51] We argue that the medium-range ordering mechanism relating to this secondary relaxation process plays a significant role in the long-time relaxation behavior in MG-298 annealed at 0.78 and 0.89 T_g. Present results indicate that the rearrangements of the MRO during relaxation occur heterogeneously, thus enhancing the structural/mechanical heterogeneity of MG-298. This feature of relaxation in MGs has not been observed since previous investigation of the relaxation mainly by using enthalpy or dynamic mechanical relaxation methods on liquid-quenched MGs with different local chemical orders from deposited MG.[20,52] In a Zr−Ni MG film, an annealing-induced increased degree of heterogeneity has been also observed from the width of the energy spectrum, which is related to the fractal growth of the solid-like regions.[53] Recently, it has been found that preannealing near T_g led to a shorter relaxation time in a Cu−Zr MG deposited at 0.89 T_g, different from that of the liquid quenched MG.[54] It is unclear whether the enhanced heterogeneity upon annealing observed in MG-298 also implies an acceleration of dynamics, which needs further investigation. In contrast, the slight change of stiffness distribution after annealing in MG-560 suggests that the percolating stability-favored cluster network shows a strong resistance to rearrangement (mechanical stability) at a larger length scale than for the MRO, which correlates with the enhanced T_x.

To conclude, the nature of ultrastability and optimality of 0.7−0.8 T_g in an UMG has been uncovered in terms of the enhanced degree of nanoscale-to-mesoscale heterogeneity and percolating backbone network formation of stability-favored clusters. The change of T_x and heterogeneity with T_{sub} should closely correlate with the connection of icosahedra-like clusters and the dispersity of local clusters. The ordinary-ultrastable transition of stability with a giant change of T_x in MGs can be deemed as a percolation transition in connection of the stability-favored clusters. The percolating network of such clusters suppresses the variation of heterogeneity upon annealing in the UMG. The enhanced structural/mechanical heterogeneity after annealing in MG-298 suggests a heterogeneous nature of cluster network rearrangements. The present work offers new insight into the origin of relaxation and stability of MGs and provides a step toward advanced MGs with superior stability and performances.

■ ASSOCIATED CONTENT

Ⓢ Supporting Information

The Supporting Information is available free of charge at https://pubs.acs.org/doi/10.1021/acs.nanolett.1c05039.

Experimental methods, TEM image of the as-deposited MGs, AFM images, energy dissipation maps, hardness and modulus derived from nanoindentation experiments, creep experiment from nanoindentation, creep displacement, 3-D images of stiffness of the as-deposited and annealed MGs, autocorrelation maps of the annealed MGs, percolation model, autocorrelation image of the as-deposited MG-596, autocorrelation image of the as-deposited MG-298 and MG-560 with a larger box size (PDF)

■ AUTHOR INFORMATION

Corresponding Authors

Qiang Luo − *School of Materials Science and Engineering, Jiangsu Key Laboratory for Advanced Metallic Materials, Southeast University, Nanjing 211189, China;* ⓞ orcid.org/0000-0001-5682-5536; Email: q.luo@seu.edu.cn

Baolong Shen − *School of Materials Science and Engineering, Jiangsu Key Laboratory for Advanced Metallic Materials, Southeast University, Nanjing 211189, China;* ⓞ orcid.org/0000-0002-0358-6540; Email: blshen@seu.edu.cn

Authors

Zhengguo Zhang − *School of Materials Science and Engineering, Jiangsu Key Laboratory for Advanced Metallic Materials, Southeast University, Nanjing 211189, China*

Donghui Li − *School of Materials Science and Engineering, Jiangsu Key Laboratory for Advanced Metallic Materials, Southeast University, Nanjing 211189, China*

Peng Luo − *Institute of Physics, Chinese Academy of Sciences, 100190 Beijing, China; University of Chinese Academy of Sciences, 100049 Beijing, China;* ⓞ orcid.org/0000-0003-4280-4990

Weihua Wang − *Institute of Physics, Chinese Academy of Sciences, 100190 Beijing, China; University of Chinese Academy of Sciences, 100049 Beijing, China;* ⓞ orcid.org/0000-0002-9155-2462

Complete contact information is available at:
https://pubs.acs.org/10.1021/acs.nanolett.1c05039

Author Contributions

Q.L. conceived the research. Q.L. fabricated the samples and performed the nanoindentation and resistance measurements. Q.L. and Z.G.Z. carried out HRTEM and HAADF-STEM experiments. D.H.L. and Q.L. conducted the annealing experiments. Q.L. and B.L.S. completed the manuscript. All authors contributed to data analysis and discussion.

Notes

The authors declare no competing financial interest.

■ REFERENCES

(1) Swallen, S. F.; Kearns, K. L.; Mapes, M. K.; Kim, Y. S.; McMahon, R. J.; Ediger, M. D.; Wu, T.; Yu, L.; Satija, S. Organic glasses with exceptional thermodynamic and kinetic stability. *Science* **2007**, *315* (5810), 353−356.

(2) Pérez-Castañeda, T.; Rodríguez-Tinoco, C.; Rodríguez-Viejo, J.; Ramos, M. A. Suppression of tunneling two-level systems in ultrastable glasses of indomethacin. *Proc. Natl. Acad. Sci. U. S. A.* **2014**, *111*, 11275−80.

(3) Kearns, K. L.; Still, T.; Fytas, G.; Ediger, M. D. High-modulus organic glasses prepared by physical vapor deposition. *Adv. Mater.* **2010**, *22*, 39−42.

(4) Kearns, K. L.; Swallen, S. F.; Ediger, M. D.; Wu, T.; Yu, L. J. Influence of substrate temperature on the stability of glasses prepared by vapor deposition. *Chem. Phys.* **2007**, *127* (15), 154702.

(5) Ishii, K.; Nakayama, H.; Hirabayashi, S.; Moriyama, R. Anomalously high-density glass of ethylbenzene prepared by vapor deposition at temperatures close to the glass-transition temperature. *Chem. Phys. Lett.* **2008**, *459* (1−6), 109−112.

(6) Nakayama, H.; Omori, K.; Inoue, K.; Ishii, K. Molar Volumes of Ethylcyclohexane and Butyronitrile Glasses Resulting from Vapor Deposition: Dependence on Deposition Temperature and Comparison to Alkylbenzenes. *J. Phys. Chem. B* **2013**, *117*, 10311.

(7) Singh, S.; Ediger, M. D.; de Pablo, J. Ultrastable glasses from in silico vapour deposition. *J. Nat. Mater.* **2013**, *12*, 139−144.

(8) Hocky, G. M.; Berthier, L.; Reichman, D. R. Equilibrium ultrastable glasses produced by random pinning. *J. Chem. Phys.* **2014**, *141*, 224503.

(9) Dalal, S. S.; Walters, D. M.; Lyubimov, I.; de Pablo, J. J.; Ediger, M. D. Tunable molecular orientation and elevated thermal stability of vapor-deposited organic semiconductors. *Proc. Natl. Acad. Sci. U. S. A.* **2015**, *112*, 4227−4232.

(10) Dalal, S. S.; Fakhraai, Z.; Ediger, M. D. High-throughput ellipsometric characterization of vapor-deposited indomethacin glasses. *J. Phys. Chem. B* **2013**, *117*, 15415−15425.

(11) Guo, Y.; Morozov, A.; Schneider, D.; Chung, J. W.; Zhang, C.; Waldmann, M.; Yao, N.; Fytas, G.; Arnold, C. B.; Priestley, R. D. Ultrastable nanostructured polymer glasses. *Nat. Mater.* **2012**, *11*, 337−43.

(12) Yu, H.-B.; Luo, Y.; Samwer, K. Ultrastable metallic glass. *Adv. Mater.* **2013**, *25*, 5904−5908.

(13) Wang, J. Q.; Shen, Y.; Perepezko, J. H.; Ediger, M. D. Increasing the kinetic stability of bulk metallic glasses. *Acta Mater.* **2016**, *104*, 25−32.

(14) Magagnosc, D. J.; Fang, G.; Yu, L.; Cheng, X. M.; Gianola, D. S. Isochemical control over structural state and mechanical properties in Pd-based metallic glass by sputter deposition at elevated temperatures. *APL Mater.* **2016**, *4*, 086104.

(15) Ngai, K. L.; Wang, L. M.; Yu, H. B. Relating Ultrastable Glass Formation to Enhanced Surface Diffusion via the Johari-Goldstein β-Relaxation in Molecular Glasses. *J. Phys. Chem. Lett.* **2017**, *8*, 2739−2744.

(16) Liu, S. Y.; Cao, Q. P.; Qian, X.; Wang, C.; Wang, X. D.; Zhang, D. X.; Hu, X. L.; Xu, W.; Ferry, M.; Jiang, J. Z. Effects of substrate temperature on structure, thermal stability and mechanical property of a Zr-based metallic glass thin film. *Thin Solid Films* **2015**, *595*, 17.

(17) Chu, J.-H.; Chen, H.-W.; Chan, Y.-C.; Duh, J.-G.; Lee, J.-W.; Jang, J.S.-C. Modification of structure and property in Zr-based thin film metallic glass via processing temperature control. *Thin Solid Films* **2014**, *561*, 38.

(18) Yu, P.; Bai, H. Y.; Tang, M. B.; Wang, W. L. Excellent glass-forming ability in simple $Cu_{50}Zr_{50}$-based alloys. *J. Non-Cryst. Solids* **2005**, *351*, 1328−1332.

(19) Luo, P.; Cao, C. R.; Zhu, F.; Lv, Y. M. Ultrastable metallic glasses formed on cold substrates. *Nat. Commun.* **2018**, *9*, 1389.

(20) Bokas, G. B.; Zhao, L.; Morgan, D.; Szlufarska, I. Increased stability of CuZrAl metallic glasses prepared by physical vapor deposition. *J. Alloys Compd.* **2017**, *728*, 1110.

(21) Zhu, F.; Nguyen, H. K.; Song, S. X.; Aji; Daisman, P. B.; Hirata, A.; Wang, H.; Nakajima, K.; Chen, M. W. Intrinsic correlation between β-relaxation and spatial heterogeneity in a metallic glass. *Nat. Commun.* **2016**, *7*, 11516.

(22) Aji, D. P. B.; Hirata, A.; Zhu, F.; Liu, P.; Reddy, K. M.; Song, S. X.; Liu, Y. H.; Fujita, T.; Kohara, S. J.; Chen, M. W. Ultrastrong and Ultrastable Metallic Glass. *arXiv:1306.1575* **2013**, https://arxiv.org/abs/1306.1575.

(23) Berthier, L.; Charbonneau, P.; Flenner, E.; Zamponi, F. Origin of Ultrastability in Vapor-Deposited Glasses. *Phys. Rev. Lett.* **2017**, *119*, 188002.

(24) Sheng, H. W.; Luo, W. K.; Alamgir, F. M.; Bai, J. M.; Ma, E. Atomic packing and short-to-medium range order in metallic glasses. *Nature (London)* **2006**, *439*, 419−425.

(25) Chen, D. Z.; Shi, C. Y.; An, Q.; Zeng, Q. S.; Mao, W. L.; Goddard, W. A.; Greer, J. R. Fractal atomic-level percolation in metallic glasses. *Science* **2015**, *349*, 1306−1310.

(26) Ma, D.; Stoica, A. D.; Wang, X. L. Power-law scaling and fractal nature of medium-range order in metallic glasses. *Nat. Mater.* **2009**, *8*, 30−34.

(27) Huang, B.; Ge, T.P.; Liu, G.L.; Luan, J.H.; He, Q.F.; Yuan, Q.X.; Huang, W.X.; Zhang, K.; Bai, H.Y.; Shek, C.H.; Liu, C.T.; Yang, Y.; Wang, W.H. Density fluctuations with fractal order in metallic glasses detected by synchrotron X-ray nano-computed tomography. *Acta Mater.* **2018**, *155*, 69−79.

(28) Yang, Y.; Zhou, J. H.; Zhu, F.; Yuan, Y. K.; Chang, D. J.; Kim, D. S.; Pham, M.; Rana, A.; Tian, X. Z.; Yao, Y. G.; Osher, S. J.; Schmid, A. K.; Hu, L. B.; Ercius, P.; Miao, J. W. Determining the three-dimensional atomic structure of an amorphous solid. *Nature* **2021**, *592*, 60−64.

(29) Yu, H.-B.; Richert, R.; Samwer, K. Structural rearrangements governing Johari-Goldstein relaxations in metallic glasses. *Sci. Adv.* **2017**, *3*, e1701577.

(30) Wang, X. D.; Jiang, Q. K.; Cao, Q. P.; Bednarcik, J.; Franz, H.; Jiang, J. Z. Atomic structure and glass forming ability of $Cu_{46}Zr_{46}Al_8$ bulk metallic glass. *J. Appl. Phys.* **2008**, *104*, 093519.

(31) Fang, H. Z.; Hui, X.; Chen, G. L.; Liu, Z. K. Al-centered icosahedral ordering in $Cu_{46}Zr_{46}Al_8$ bulk metallic glass. *Appl. Phys. Lett.* **2009**, *94*, 091904.

(32) Zhu, F.; Hirata, A.; Liu, P.; Song, S. X.; Tian, Y.; Han, J. H.; Fujita, T.; Chen, M. W. Phys. Correlation between local structure

order and spatial heterogeneity in a metallic glass. *Rev. Lett.* **2017**, *119*, 215501.

(33) Li, W. Z.; Wang, C. Z.; Hao, S. G.; Kramer, W. J.; Ho, K. M. Structural heterogeneity and medium-range order in Zr_xCu_{100-x} metallic glasses. *Phys. Rev. B* **2009**, *80*, 184201.

(34) Soklaski, R.; Nussinov, Z.; Markow, Z.; Kelton, K. F.; Yang, L. Connectivity of the Icosahedral Network and a Dramatically Growing Static Length Scale in Cu-Zr Binary Metallic Glasses. *Phys. Rev. B* **2013**, *87*, 184203.

(35) Hu, Y. C.; Li, F. X.; Li, M. Z.; Bai, H. Y.; Wang, W. H. Five-fold symmetry as indicator of dynamic arrest in metallic glass-forming liquids. *Nat. Commun.* **2015**, *6*, 8310.

(36) Tsai, P.; Kranjc, K.; Flores, K. M. Hierarchical heterogeneity and an elastic microstructure observed in a metallic glass alloy. *Acta Mater.* **2017**, *139*, 11−20.

(37) Wagner, H.; Bedorf, D.; Kuchemann, S.; Schwabe, M.; Zhang, B.; Arnold, W.; Samwer, K. Local elastic properties of a metallic glass. *Nat. Mater.* **2011**, *10*, 439−442.

(38) Ross, P.; Kuchemann, S.; Derlet, P. M.; Yu, H. B.; Arnold, W.; Liaw, P.; Samwer, K.; Maass, R. Linking macroscopic rejuvenation to nano-elastic fluctuations in a metallic glass. *Acta Mater.* **2017**, *138*, 111−118.

(39) Fan, G. Y.; Cowley, J. M. Auto-correlation analysis of high resolution electron micrographs of near-amorphous thin films. *Ultramicroscopy* **1985**, *17*, 345−356.

(40) Dawson, K. J.; Kearns, K. L.; Yu, L.; Steffen, W.; Ediger, M. D. Physical vapor deposition as a route to hidden amorphous states. *Proc. Natl. Acad. Sci. U.S.A.* **2009**, *106*, 15165−15170.

(41) Zhou, C.; Hu, U.; Sun, Q. J.; Qin, J. Y.; Bian, X. F.; Yue, Y. Z. Indication of liquid-liquid phase transition in CuZr-based melts. *Appl. Phys. Lett.* **2013**, *103* (17), 171904.

(42) Zhao, X.; Wang, C.; Zheng, H. J.; Tian, Z.; Hu, L. The role of liquid-liquid transition in glass formation of CuZr alloys. *Phys. Chem. Chem. Phys.* **2017**, *19* (24), 15962−15972.

(43) Zhou, C.; Hu, L.; Sun, Q. J.; Zheng, H. J.; Zhang, C. Z.; Yue, Y. Z. structural evolution during fragile-to-strong transition in CuZr(Al) glass-forming liquids. *J. Chem. Phys.* **2015**, *142* (6), 064508.

(44) Li, M. X.; Sun, Y. T.; Wang, C.; Hu, L. W.; Sohn, S.; Schroers, J.; Wang, W. H.; Liu, Y. H. Data-driven discovery of a universal indicator for metallic glass forming ability. *Nat. Mater.* **2022**, *21*, 165.

(45) Pan, J.; Wang, Y. X.; Guo, Q.; Zhang, D.; Greer, A. L.; Li, Y. Extreme rejuvenation and softening in a bulk metallic glass. *Nat. Commun.* **2018**, *9*, 560.

(46) Ketov, S. V.; Sun, Y. H.; Nachum, S.; Lu, Z.; Checchi, A.; Beraldin, A. R.; Bai, H. Y.; Wang, W. H.; Louzguine-Luzgin, D. V.; Carpenter, M. A.; Greer, A. L. Rejuvenation of metallic glasses by non-affine thermal strain. *Nature* **2015**, *524*, 200−203.

(47) Concustell, A.; Méar, F. O.; Suriñach, S.; Baró, M. D.; Greer, A. L. Structural relaxation and rejuvenation in a metallic glass induced by shot-peening. *Philos. Mag. Lett.* **2009**, *89*, 831−840.

(48) Taub, A. I.; Spaepen, F. The kinetics of structural relaxation of a metallic glass. *Acta Metall.* **1980**, *28*, 1781−1788.

(49) Ruta, B.; Chushkin, Y.; Monaco, G.; Cipelletti, L.; Pineda, E.; Bruna, P.; Giordano, V. M.; Gonzalez-Silveira, M. Atomic-scale relaxation dynamics and ageing in a metallic glassprobed by x-ray photon correlation spectroscopy. *Phys. Rev. Lett.* **2012**, *109*, 165701.

(50) Fan, Y.; Iwashita, T.; Egami, T. Crossover from localized to cascade relaxations in metallic glasses. *Phys. Rev. Lett.* **2015**, *115*, 045501.
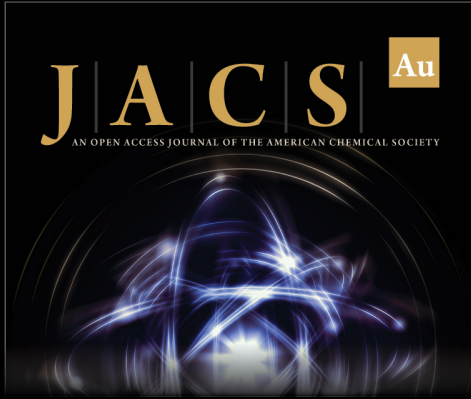
(51) Giordano, V. M.; Ruta, B. Unveiling the structural arrangements responsible for the atomic dynamics in metallic glasses during physical ageing. *Nat. Commun.* **2016**, *7*, 10344.

(52) Qiao, J. C.; Feng, S. D.; Pelletier, J. M.; Crespo, D.; Pineda, E.; Yao, Y. Physical ageing effects on the dynamic relaxation behavior and mechanical properties of $Cu_{46}Zr_{46}Al_8$ metallic glass. *J. Alloys Compd.* **2017**, *726*, 195−200.

(53) Yang, Y.; Zeng, J. F.; Volland, A.; Blandin, J. J.; Gravier, S.; Liu, C. T. Fractal growth of the dense-packing phase in annealed metallic glass imaged by high-resolution atomic force microscopy. *Acta Mater.* **2012**, *60*, 5260−5272.

(54) Luttich, M.; Giordano, V. M.; Le Floch, S.; Pineda, E.; Zontone, F.; Luo, Y. S.; Samwer, K.; Ruta, B. Anti-ageing in Ultrastable Metallic Glasses. *Phys. Rev. Lett.* **2018**, *120*, 135504.